FLASHING: New high-velocity H2O masers in IRAS 18286−0959

Hiroshi Imai [1,2,3,*] Yuri Uno,[3] Daichi Maeyama,[4] Ryosuke Yamaguchi,[4]
Kei Amada,[3] Yuhki Hamae,[4] Gabor Orosz,[5,6] José F. Gómez,[7]
Daniel Tafoya,[8,9] Lucero Uscanga,[10] and Ross A. Burns [8,11]

[1] Amanogawa Galaxy Astronomy Research Center, Graduate School of Science and Engineering, Kagoshima University, 1-21-35 Korimoto, Kagoshima, Kagoshima 890-0065, Japan

[2] Center for General Education, Institute for Comprehensive Education, Kagoshima University, 1-21-30 Korimoto, Kagoshima, Kagoshima 890-0065, Japan

[3] Department of Physics and Astronomy, Graduate School of Science and Engineering, Kagoshima University, 1-21-35 Korimoto, Kagoshima, Kagoshima 890-0065, Japan

[4] Department of Physics and Astronomy, Faculty of Science, Kagoshima University, 1-21-35 Korimoto, Kagoshima, Kagoshima 890-0065, Japan

[5] School of Natural Sciences, University of Tasmania, Private Bag 37, Hobart, Tasmania 7001, Australia

[6] Xinjiang Astronomical Observatory, Chinese Academy of Sciences, 150 Science 1-Street, Urumqi, Xinjiang 830011, China

[7] Instituto de Astrofísica de Andalucía, CSIC, Glorieta de la Astronomía s/n, E-18008 Granada, Spain

[8] National Astronomical Observatory of Japan, 2-21-1 Osawa, Mitaka, Tokyo, 181-8588, Japan

[9] Department of Space, Earth and Environment, Chalmers University of Technology, Onsala Space Observatory, 439 92 Onsala, Sweden

[10] Departamento de Astronomía, Universidad de Guanajuato, A.P. 144, 36000 Guanajuato, Gto., Mexico

[11] Korea Astronomy and Space Science Institute, 776 Daedeokdae-ro, Yuseong-gu, Daejeon 34055, Republic of Korea

*E-mail: k3830453@kadai.jp

Abstract

We discovered new high-velocity components of H_2O maser emission in one of the "water fountain" sources, IRAS 18286−0959, which has been monitored using the Nobeyama 45 m telescope in the FLASHING (Finest Legacy Acquisitions of SiO- and H_2O-maser Ignitions by Nobeyama Generation) project since 2018 December. The maser spectra show new components with extremely high expansion velocities ($>200\,\mathrm{km\,s^{-1}}$ projected in the line of sight), some of which are located symmetrically in the spectrum with respect to the systemic velocity. They were also mapped with KaVA (KVN and VERA Combined Array) in 2019 March. We located some of these maser components closer to the central stellar system than other high-velocity components (50–$200\,\mathrm{km\,s^{-1}}$) that have been confirmed to be associated with the known bipolar outflow. The new components would have flashed in the fast collimated jet at a speed of over $300\,\mathrm{km\,s^{-1}}$ (soon) after 2011 when they had not been detected. The fastest of the new components seem to indicate rapid deceleration in these spectra; however, our present monitoring is still too sparse

to unambiguously confirm it (up to $50\,km\,s^{-1}\,yr^{-1}$) and too short to reveal their terminal expansion velocity, which will be equal to the expansion velocity that has been observed ($v_{exp} \sim 120\,km\,s^{-1}$). Future occurrences of such extreme-velocity components may provide a good opportunity to investigate possible recurrent outflow ignitions. Thus, the sculpture of the parental envelope will be traced by the dense gas that is entrained by the fast jet and exhibits spectacular distributions of the relatively stable maser features.

Key words: masers — stars: AGB and post-AGB — stars: individuals (IRAS 18286−0959)

1 Introduction

Our understanding of the final stellar evolution, exhibiting copious and inhomogeneous mass loss and the subsequent formation of planetary nebulae (PNe) with a wide variety of morphologies, remains incomplete. It is considered that such transformations will happen during a relatively short period, from the end of the asymptotic giant branch (AGB) phase of stellar evolution to the beginning of the post-AGB phase, when an AGB stellar wind rapidly develops a circumstellar envelope (CSE) (e.g., Lewis 2001). It has been confirmed that highly collimated, fast jets will be newly ejected from some of these stars (e.g., Sahai & Trauger 1998). These jets shape the previously ejected CSE, so they may be ultimately responsible for the final morphologies of PNe. However, two open questions remain: the launching mechanism and the timescale of such jet ejections.

"Water fountain" (WF) sources have been identified as AGB or post-AGB stars hosting fast bipolar jets traced by H_2O maser emission (Imai 2007). WF candidates were first confirmed in maser spectra with extreme velocity widths, much larger than those of typical 1612 MHz OH maser emission, exhibiting clear double-horned spectral profiles ($10–20\,km\,s^{-1}$; e.g., Likkel et al. 1992; cf. Engels & Bunzel 2015). Only 15 WFs have been confirmed to date (Gómez et al. 2017), implying an extremely short timescale of the phase when such high-velocity circumstellar H_2O masers are visible (<100 yr; Imai 2007). Interferometric observations of these H_2O masers show a wide variety of spatio-kinematical structures for the masers, reflecting different types of central stellar systems driving these jets and/or different stages of jet evolution. The diversity of the central star properties is indicated by the variety of substructures in the maser spatio-kinematics such as multiple arcs, pairs of maser feature groups distributed point-symmetrically, groups of maser features containing a large internal velocity dispersion ($\gg 10\,km\,s^{-1}$; e.g., Imai et al. 2002; Claussen et al. 2009; Imai et al 2013b; Orosz et al. 2019).

The temporal evolution of each jet can also be monitored in the cases where its growth rate, namely the change rate of the total length of the maser jet on the sky, is consistent with the mean of the proper motion speeds of the individual maser features (Imai et al. 2007; Chong et al. 2015). Recent observations of thermal molecular lines and dust emission with the Atacama Large Millimeter-and-submillimeter Array (ALMA) have elucidated the complete spatio-morphologies of WF sources (e.g., Sahai et al. 2017; Tafoya et al. 2019, 2020). In some WFs, H_2O masers are suggested to trace the interaction of the fast jet with the parental CSE sculpted by the jet, and the resulting deceleration of the jet that leads entrained material along the jets. The jet deceleration is suggested by the spatio-kinematics of the H_2O masers themselves (Orosz et al. 2019). However, other WFs show an opposite trend, with accelerating masers (e.g., Gómez et al. 2015), which could indicate a different nature of these WF phenomenon, maybe related to the evolutionary phase of the sources.

Taking into account the rarity of WFs, their possibly rapid evolution, and the possibility of the appearance of new H_2O masers in the known WFs and WF candidates, monitoring of these H_2O masers in single-dish observations with moderate cadence (1–8 weeks) is crucial for understanding the phenomena of WFs in a unified scheme. The possible deceleration of the jets may be proved by detecting H_2O masers at higher velocities with decreasing velocity drifts. Periodic behavior of the maser spectrum may indicate either periodic ejections of jets or pulsation of the central evolved star. In the latter case, synergistic monitoring of 1612 MHz OH masers and SiO (in addition to H_2O) masers will provide more concrete evidence for the stellar pulsation (e.g., Herman & Habing 1985). The weakness of some velocity components of H_2O masers in WFs requires highly sensitive telescopes for systematic monitoring observations, and possibly an internationally coordinated program that can manage regular monitoring activities for the known WFs and WF candidates. The Nobeyama 45 m telescope is one of the best-suited telescopes for such monitoring observations thanks to its dynamic scheduling,[1] which provided good opportunities for high-sensitivity H_2O maser observations. Moreover, the new quasi-optics enables us to simultaneously observe H_2O and SiO masers (Okada et al. 2020). We have therefore monitored the WFs in the FLASHING

---

[1] Dynamic scheduling as the back-up program was conducted until 2019 May.

Table 1. Summary of the FLASHING observations toward IRAS 18286−0959.

Epoch (yy/mm/dd)	T_{sys}* (K)	t_{int}† (m)	Noise‡ (mJy)
18/12/23	∼150	18	118
19/01/05	∼110	106	32
19/02/06	∼150	47	77
19/03/06	∼130	35	78
19/04/15	∼190	58	114
19/04/28	∼130	39	56
19/05/14	∼170	37	108
19/05/29	∼230	152	81
19/12/06	∼120	28	77
19/12/20	∼100	49	53
20/01/10	∼110	23	74

*System noise temperature.

†On-source integration time.

‡One-σ noise level of the spectrum.

(Finest Legacy Acquisitions of SiO and H_2O maser Ignitions by Nobeyama Generation) project since 2018 December.

In this paper we report the first scientific results of FLASHING, yielded for IRAS 18286−0959 (hereafter abbreviated as I18286). H_2O masers in I18286 have been mapped in several very long baseline interferometry (VLBI) observations using the Very Long Baseline Array (VLBA) and the VLBI Exploration of Radio Astrometry (VERA; Yung et al. 2011, Paper I; Imai et al. 2013a, Paper II; Imai et al. 2013c, Paper III). Paper I modeled the H_2O masers on a double helix pattern. Paper II determined the trigonometric parallax distance to I18286 to be $3.61^{+0.63}_{-0.47}$ kpc. Paper III determined the locations of 1612 MHz OH masers and the low-velocity (∼10 km s^{-1}) components of the H_2O masers in the H_2O maser maps, both of which may be associated with a relic CSE in I18286. Before 2010, the H_2O masers in I18286 covered a velocity range of $-60 \leq V_{LSR} \leq 180$ km s^{-1} with respect to the local standard of rest (LSR). Yung et al. (2013) found new velocity components in 2011 around $V_{LSR} \sim -90$ and 230 km s^{-1}. This paper focuses on even newer, faster velocity components (surpassing the previously detected velocity range), found with our monitoring in FLASHING.

2 Observations and data reduction

2.1 FLASHING observations

While FLASHING is still active, in this paper we present the observed spectra towards I18286 until 2020 January 10. This data set consists of eleven epochs: eight between 2018 December and 2019 May, and three additional epochs after 2019 November. Table 1 gives a summary of the single-dish observations. We employed the new quasi-optics that

enabled us to simultaneously observe line emission at the frequency bands around 22.2 and 43.0 GHz (Okada et al. 2020), including the maser lines of H_2O $J_{K_- K_+} = 6_{12} \rightarrow 5_{23}$ at the rest frequency of 22.235080 GHz and SiO $J = 1 \rightarrow 0$ ($v = 3, 2, 1$, and 0) at 42.5–43.4 GHz. This paper shows only the H_2O maser spectra because only this maser line was detected toward I18286.

The aperture efficiency of the telescope is 0.65, yielding a flux-density conversion factor of 2.67 Jy K^{-1}, when employing the new quasi-optics. The flux density scale was obtained from the system noise temperature measured with the chopper-wheel method. The maser emission was received in both left- and right-hand circular polarizations. Position switching was employed by alternating observations of a target maser and a blank sky position for an integration time of 30 s per scan. Three spectral windows were set to cover a bandwidth of 31.25 MHz in each window, centered at the mean velocity of the maser emission in the LSR frame (∼65 km s^{-1}) and those higher and lower by 30 MHz than the first one. The SAM45 spectrometers were used to obtain 4096 spectral channels per spectral window, but the final spectra had 2048 spectral channels after smoothing. The three spectral windows cover a velocity width of 1258 km s^{-1} in total, with a velocity resolution of 0.42 km s^{-1}.

The data reduction was performed using the Java NEW-STAR software,[2] in which integration and baseline subtraction were performed in order to obtain the final maser spectra. Dependent on system noise temperature and integration time, the 1σ noise level of the spectra ranged from 32 to 118 mJy. We identified detections of spectral components if their flux density was higher than the 5σ noise level (160–990 mJy). We then identified each spectral peak if it was composed of three or more detected components in consecutive spectral channels. In the case of multiple peaks, which are close in velocity and thus blended together, each peak was identified as an independent peak if its flux density was higher by 3σ than that of the spectral channel of the tail of a contiguous intersecting peak.

2.2 KaVA mapping observation

The H_2O masers in I18286 were also observed on 2019 March 4 for 6 hr with KaVA, an array composed of four telescopes of the Japanese VERA array plus three of the Korean VLBI Network (KVN). The fringe finder OT 081 and the delay calibrator J183005.9+061915 were also observed three times, every 25 min. These sources were observed in both left- and right-hand circular

---

[2] See the NEWSTAR home page ⟨https://www.nro.nao.ac.jp/∼nro45mrt/html/obs/newstar/index.html⟩.

polarizations with the KVN telescopes, but only the former polarization data were valid. With VERA, only the left-hand circular polarization was observed, but the dual-beam system allowed simultaneous observations of our target and the position reference source J183220.8−103511 (hereafter J1832). The received signals were filtered into two base-band channels (BBCs), each with a bandwidth of 128 MHz, and recorded in 2-bit quantization, yielding a total recording rate of 1024 Mbps.

The data correlation was made using the Daejeon Correlator in the Korea–Japan Correlation Center (KJCC). The recorded signals taken with both of VERA's dual beams were correlated with those with the KVN telescopes. Two correlated data sets were provided from the two BBCs, one including the maser source and the other J1832. The BBC observing I18286 contained 4096 spectral channels, yielding a velocity channel spacing of 0.42 km s^{-1}, while there were 128 spectral channels for the other BBC observing J1832. Note that the latter data were invalid in the VERA–KVN baselines for the scans on J1832.

The data reduction was performed using NRAO AIPS with Python scripts and the ParselTongue package.[3] Standard a priori calibration procedures were performed to calibrate the visibility amplitudes using antenna gain and system noise temperature information. The delay calibration was performed using the scans on J183005.9+061915. Fringe fitting and self-calibration were performed using the data in a reference spectral channel at an LSR velocity of 139.5 km s^{-1}, which included a bright and compact maser spot. The positional offsets of the maser spots given in this paper are referred to the position of this reference spot. Image cubes of the maser emission were created using the CLEAN deconvolution algorithm with a Gaussian synthesized beam of 2.1 × 1.4 mas at a position angle of −18°, yielding a 1σ noise level of ∼20 mJy in spectral channels without bright maser spots. Maser spots brighter than a 7σ noise level were identified in the individual spectral channels and grouped into isolated maser features, each of which includes maser spots located within 1–2 mas in position along consecutive spectral channels. We assume that the individual maser features correspond to physical features or gas clumps emitting the masers.

The visibility data of J1832 observed only with VERA as well as the maser data were used for precise astrometry of the maser source. These visibilities were calibrated using a more precise delay-tracking model. The data of the calibrator scans were used for instrumental delay calibration, including that for relative delay and phase offsets between VERA's dual beams. The fringe fitting and

self-calibration solutions obtained from the maser scans as mentioned above were applied to the J1832 data, yielding the relative position of J1832 with respect to that of the reference maser spot. However, the astrometric accuracy of ∼0.4 mas is poorer than expected (<0.1 mas). This is a trade-off of the wide velocity coverage in the full KaVA array for the maser data instead of more accurate astrometry with VERA. The former observation setup yielded less sensitivity for J1832 in VERA, while the latter a limited velocity coverage of the maser source with the full KaVA. The self-calibration solutions taken from the maser data were also imperfect for astrometry due to insufficient performance of KVN, whose accurate information for the station coordinates was still unavailable.

3 Results

3.1 Maser spectra

Figure 1 shows the spectra of H_2O masers in I18286 taken in the first eight epochs of FLASHING. They clearly show new components in $V_{LSR} < -60$ km s^{-1} and $V_{LSR} > 200$ km s^{-1}, which had not been identified in the previous observations during 2006 April–2010 April (Deguchi et al. 2007; Paper I). In our observations, we also find that the velocity components in the velocity range of $V_{LSR} = 130$–160 km s^{-1} are flaring compared to those seen in the previous observations by a factor of up to four.

The central velocity between the two extremely high velocity components present in all observing sessions (found around $V_{LSR} \sim -150$ and 240 km s^{-1}) is V_{LSR}(center) $\simeq$ 45 km s^{-1}, close to the velocity of the CO $J = 3 \rightarrow 2$ emission ($V_{LSR} \simeq 65$ km s^{-1}; Imai et al. 2009) and the velocity of the single 1612 MHz OH maser component in I18286 [V_{LSR}(OH) ~ 40 km s^{-1}; Paper III]. In evolved stars, OH masers at 1612 MHz usually show a double-horned profile, tracing an expansion of the CSE. Here we suggest that the central velocity of the CO emission traces the systemic stellar velocity ($V_* \simeq 65$ km s^{-1}), while the velocity difference between the CO and OH peaks represents the expansion velocity of the relic envelope ($V_{expansion} \simeq 25$ km s^{-1}). Furthermore, we found even higher-velocity red-shifted components at $V_{LSR} \simeq 345$ and 336 km s^{-1} in the spectra on 2019 February 6 and May 14, respectively. As discussed later, it is unclear whether these represent the same gas clump (undergoing rapid deceleration, and a temporary maser quench between 2019 March and April), or are independent clumps. In the latter case, each of the clumps would be short lived (>2 months).

The maximum velocity separation between the fastest maser component (345 km s^{-1}) and the systemic velocity is $\simeq$280 km s^{-1}). This is much larger than the expansion

---

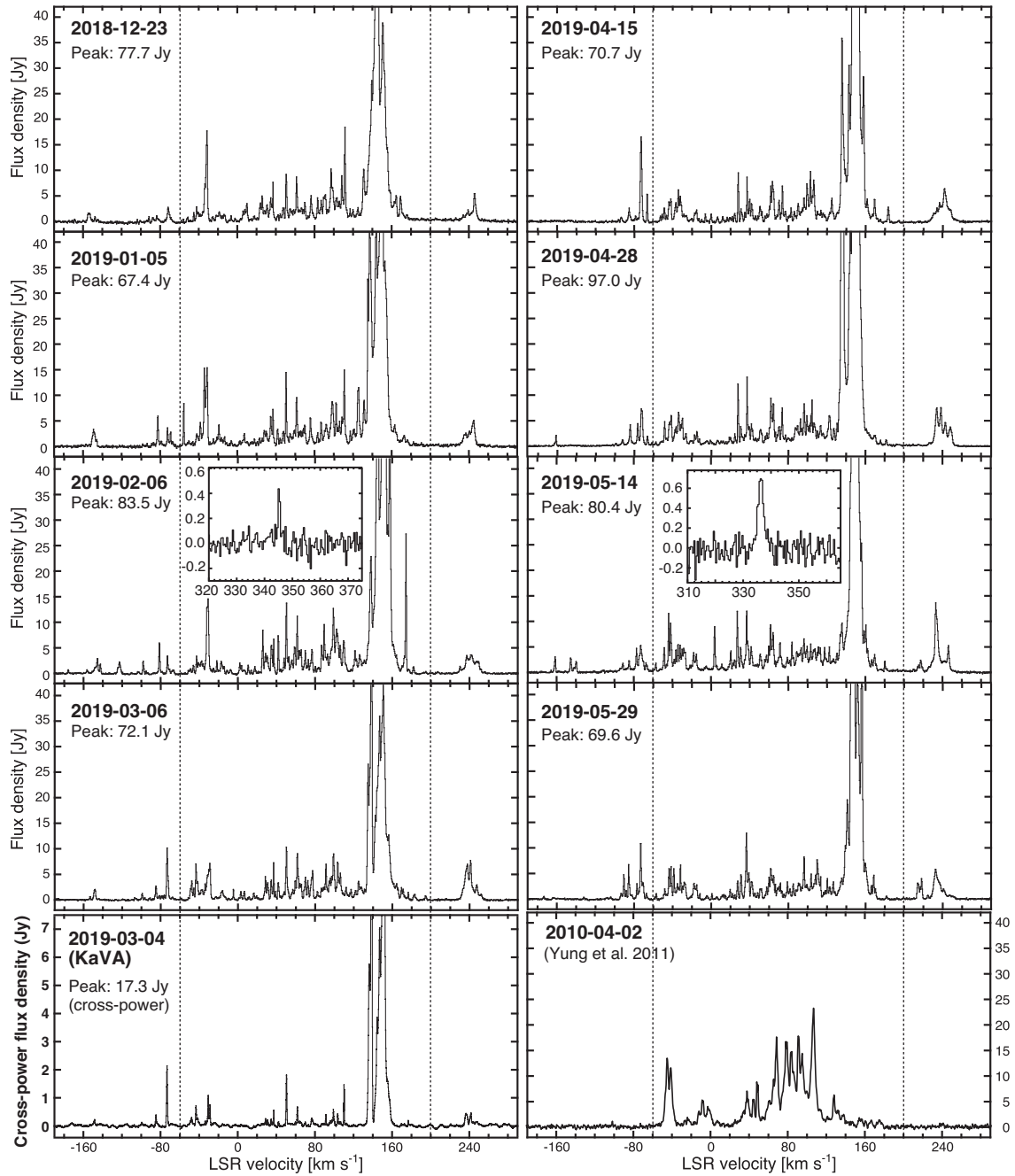[3] See the ParselTongue wiki ⟨http://www.jive.nl/jivewiki/doku.php?id=parseltongue:parseltongue⟩.

Fig. 1. Time series of the H_2O maser spectra taken toward IRAS 18286−0959 using the Nobeyama 45 m telescope from 2018 December 23 to 2019 May 29. The insets of the spectra on 2019 February 6 and May 14 show the zoomed spectra of the further high-velocity maser components detected at $V_{LSR} \approx 336$ and $345\,km\,s^{-1}$. For comparison, the spectra taken on 2010 April 2 cited from Paper I are displayed in the bottom right panel with the same vertical scale as for the 45 m spectra. The scalar-averaging cross-power spectrum taken in the KaVA observation is displayed in the bottom left panel. The two vertical dotted lines indicate LSR velocities of −60 and $200\,km\,s^{-1}$, over which the new high-velocity maser components appeared in the present observations.

velocity of the relic envelope mentioned above. Instead, we consider it as the lower limit of the projected jet velocity along the line of sight. This makes it one of the fastest water fountains, similar to IRAS 18113−2503 (hereafter I18113) (Gómez et al. 2011; Orosz et al. 2019). Adopting the distance to I18286 ($D = 3.6\,kpc$) and the maximum

proper motion of the H_2O masers in the jet ($\sim 10\,mas\,yr^{-1}$), the deprojected velocity of the jet would be $\sim 330\,km\,s^{-1}$ at an inclination angle of $\sim 30°$ with respect to the line of sight.

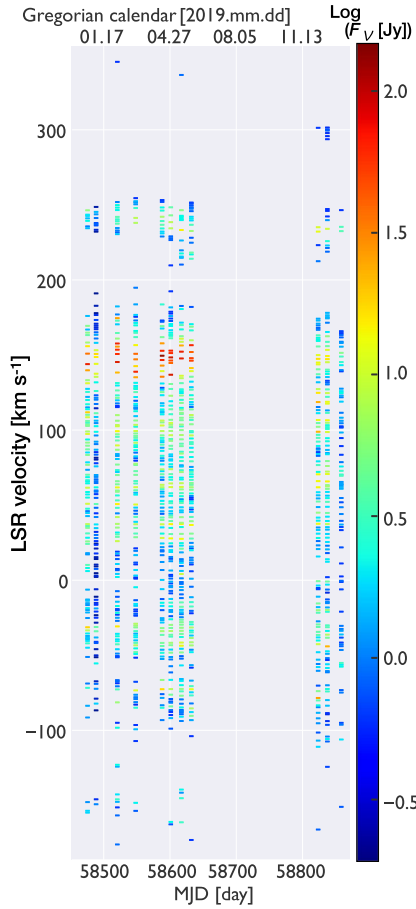Figure 2 shows the time series of velocity distributions of the identified maser peaks. The time baseline of the

Fig. 2. Velocity distributions of the spectral peaks ($>5\sigma$) of the IRAS 18286−0959 H_2O masers for the 11 epochs. A logarithm of the flux density of each spectral peak is indicated by the right-side color-scale bar.

FLASHING observations is still too short to trace any periodic variation in brightness or systematic drifts of the line-of-sight velocities of the maser peaks. It is also too short to relate the maser flare around $V_{LSR} = 130$–160 km s^{-1} with the new extremely high velocity components. One can see their large velocity drifts over one year; however, it is unclear whether the components at $V_{LSR} \simeq 345$ km s^{-1} on 2019 February 6, $\simeq 345$ km s^{-1} on 2019 May 14, and ~ 300 km s^{-1} in 2019 December–2020 January were really the same feature. Similarly, one can also note a velocity drift of the maser component at $V_{LSR} \sim -176$ km s^{-1} on 2019 February 6, ~ -173 km s^{-1} on 2019 May 29, and ~ -166 km s^{-1} on 2019 December 6.

3.2 Distribution of the maser features

Table 2 gives the parameters of the I18286 H_2O maser features detected in the KaVA image cubes. The individual rows show, respectively, the LSR velocity at the intensity

Table 2. H_2O maser features detected with KaVA.

V_{LSR}	X	σ_X	Y	σ_Y	I_{peak}	ΔV
−153.57	−80.64	0.25	117.44	0.50	0.12	0.84
−148.22	−86.16	0.09	121.15	0.10	0.72	3.16
−144.32	−86.59	0.13	113.39	0.11	0.17	0.63
−99.16	−84.99	0.06	109.08	0.09	0.55	1.26
−91.20	−85.06	0.05	109.63	0.13	0.35	0.84
−84.60	−98.09	0.06	179.46	0.09	1.18	2.32
−73.14	−102.67	0.02	182.60	0.02	3.49	2.32
−47.55	−93.18	0.18	256.19	0.11	0.80	2.95
−43.08	−91.94	0.19	256.16	0.12	1.33	6.11
−37.15	−95.23	0.20	251.61	0.10	0.26	1.47
−33.51	−90.69	0.07	256.88	0.12	0.61	2.11
−31.29	−95.45	0.07	251.87	0.09	0.56	0.63
−30.42	−100.15	0.05	179.59	0.09	1.34	1.05
−28.68	−95.74	0.12	252.00	0.10	1.11	1.69
−28.65	−100.54	0.11	243.10	0.11	0.56	2.53
−4.21	−95.82	0.10	179.80	0.05	0.36	0.63
3.59	−69.07	0.08	156.41	0.06	0.45	1.90
6.87	−68.95	0.08	156.23	0.14	0.24	1.26
17.07	−92.67	1.21	178.60	0.35	0.37	2.74
19.39	−53.75	0.09	205.44	0.11	0.23	0.63
27.17	−101.41	0.08	150.62	0.18	0.21	0.63
28.93	−81.87	0.06	88.11	0.36	0.99	4.00
34.97	−81.64	0.47	90.45	0.66	0.80	1.26
37.29	−82.59	0.12	91.21	0.23	0.43	1.47
37.52	−55.05	0.05	231.91	0.08	1.35	0.84
39.19	−82.44	0.13	90.83	0.09	0.32	0.63
42.17	−82.94	0.05	92.29	0.10	0.79	1.69
50.75	−5.43	0.02	10.23	0.04	2.83	2.11
60.02	−58.33	0.05	68.19	0.11	0.54	0.84
62.07	−24.43	0.09	58.00	0.17	1.14	1.26
62.09	−8.24	0.31	−184.19	0.18	0.59	0.84
64.61	−21.45	0.11	55.00	0.21	0.48	2.11
70.37	−23.38	0.30	−129.79	0.10	0.37	0.63
76.65	11.50	0.11	−33.09	0.15	0.70	2.53
78.05	−22.78	0.10	52.43	0.22	0.56	1.27
87.00	−34.51	0.20	−84.24	0.06	0.35	1.05
90.09	13.58	1.15	−26.22	0.16	0.41	0.84
91.52	2.93	0.13	7.71	0.05	1.03	1.68
91.76	−0.28	0.42	7.94	0.26	0.79	1.68
95.11	16.40	0.11	−34.72	0.11	0.49	1.05
96.26	−4.82	0.13	37.17	0.06	0.55	0.84
97.78	16.29	0.05	−34.13	0.07	0.77	2.32
99.41	−25.51	0.31	−59.97	0.09	0.59	1.05
99.46	−25.84	0.37	−59.79	0.15	0.60	1.26
99.46	−30.18	0.16	−86.37	0.06	1.34	2.95
99.47	18.93	0.61	−14.49	0.21	0.55	2.53
103.85	−25.26	0.51	−58.82	0.31	0.42	2.74
103.87	−29.62	0.31	−85.11	0.49	1.40	2.53
106.33	−5.66	0.07	35.81	0.07	0.73	2.32
106.93	−33.42	0.05	−83.59	0.04	0.86	1.27
107.31	2.58	0.15	7.48	0.14	0.35	2.32
109.50	−31.68	0.10	−86.39	0.15	0.24	0.63
112.58	2.45	0.08	7.32	0.12	0.52	1.47
116.56	15.86	0.16	−28.99	0.11	0.51	4.64
117.88	−34.86	0.08	−83.40	0.06	0.59	1.05

Table 2. (Continued)

V_{LSR}	X	σ_X	Y	σ_Y	I_{peak}	ΔV
122.20	5.33	0.08	−58.43	0.11	0.72	2.11
123.68	14.24	0.10	−109.73	0.15	0.27	1.26
125.38	14.18	0.12	−109.51	0.11	0.36	0.84
125.36	−3.66	0.08	4.29	0.17	0.24	1.47
127.19	14.84	0.12	−33.61	0.09	0.33	1.05
136.59	0.06	0.02	0.04	0.09	11.96	6.32
139.05	0.01	0.02	0.00	0.02	28.00	3.58
147.08	1.74	0.10	−5.64	0.25	5.59	6.74
151.10	9.03	0.19	−48.21	0.30	23.69	24.02
171.52	7.26	0.06	−41.01	0.09	0.47	0.84
177.03	6.37	0.11	−47.14	0.05	0.88	1.68
236.62	−4.37	0.08	15.23	0.04	1.28	7.16
241.89	−4.43	0.11	15.11	0.06	1.38	6.32
247.53	−4.84	0.19	15.25	0.06	0.84	7.80

peak, the right ascension offset and its uncertainty, the declination offset and its uncertainty, the peak intensity, and the full velocity width of the feature. Figure 3 shows the location of the H_2O maser components in I18286. These components are distributed in groups, tracing a point-symmetric structure with respect to the center, similar to W43A (Tafoya et al. 2020). In the figure, we label these symmetric groups with the same number, and with the letter a or b, depending whether they are located south or north of the center, respectively. The new extreme velocity components ($V_{LSR} \approx -150$ and $240\,\mathrm{km\,s^{-1}}$) correspond to Groups 2a and 2b. Group 2a is located close to the brightest and flared maser features (Group 4a).

Figure 4 shows a comparison between the maser feature distributions in 2006–2007, 2009, and 2019, and clarifies this secular variation. It is difficult to superimpose the maser maps in the common coordinate system precisely for comparison, because of the the uncertainty in the secular proper motion of the whole system. The astrometric information obtained in Paper II was composed of the Galactic rotation and the intrinsic motions of the individual maser features selected as position reference in the astrometry. Alternatively, the map registration shown in figure 4 has been produced by roughly referencing the possible location of the dynamical center of the outflow.

Although stream lines of the gas hosting these masers might be bent by a magnetic force as suggested elsewhere (e.g., Vlemmings et al. 2006), we suppose here that the individual maser features are moving in straight lines along the bipolar outflow or the jet driven by the stellar system. In this case, the stellar system may be located at the middle point between the new extreme velocity components, (X, Y) $\approx$ (−43, 66) [mas] from the reference feature used in self-calibration. Comparing with the maser map in 2008–2009 (figure 3 of Paper I), even without accurate astrometric
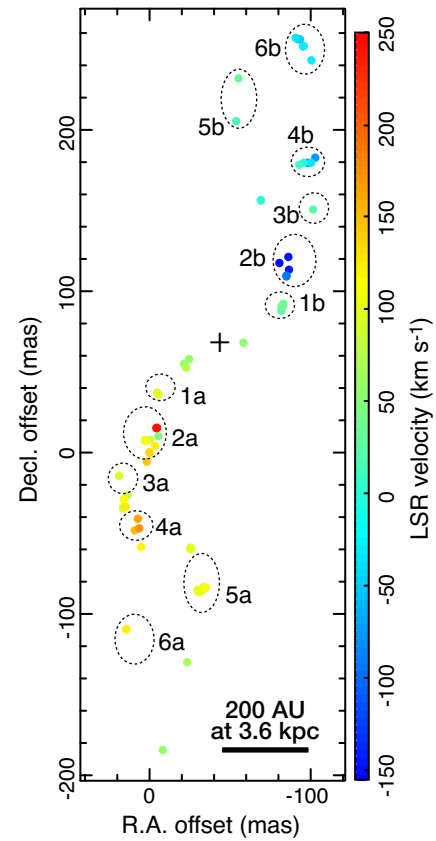

Fig. 3. Distribution of the H_2O maser features in IRAS 18286−0959 mapped with KaVA on 2019 March 4. The map origin is set to the maser spot whose emission was used for fringe fitting and self-calibration as described in the main text. The color of each filled circle indicates the LSR velocity of the maser feature, whose scale is shown in the right-side color bar. The plus symbol denotes the estimated location of the stellar system driving the outflow. The labels of the maser feature groups (from 1a/b to 6a/b) indicate point-symmetric locations of maser gas clumps with respect to the stellar system.

information, we note that the pair of extreme velocity components in the present observation are located around the same regions as the highest-velocity components in the previous observations ($V_{LSR} \approx -50$ and $160\,\mathrm{km\,s^{-1}}$; Papers I, II, III) or even slightly closer to the stellar system.

We also note that the alignment axis of the highest-velocity components seems to rotate clockwise in this observation with respect to those in the previous epochs. This clockwise rotation of the maser alignment does not agree with the expectation from the previous kinematic model of two highly collimated precessing jets (Paper I), in which the precession is counter-clockwise (with a precessing angle and period of $\sim 28°$ and $\sim 56\,\mathrm{yr}$, respectively). The spatio-kinematics of the outflow now seems to be better explained by a model of wider-angle bipolar lobes from a single driving source as proposed for W43A (Chong et al. 2015), in which H_2O masers are located along a bipolar cavity evacuated by a series of precessing collimated outflows.
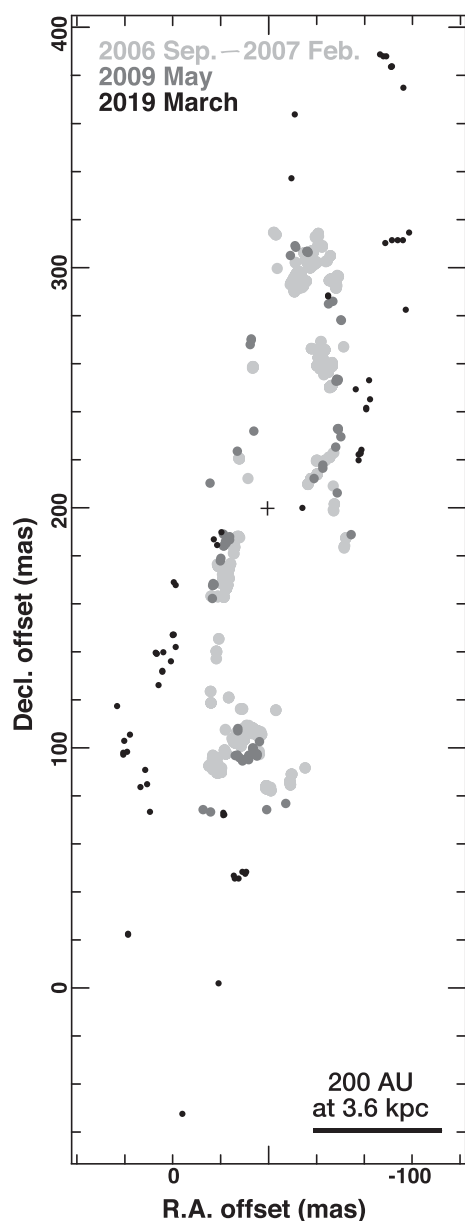
Fig. 4. Comparison of the maser feature distributions in IRAS 18286−0959. The light gray, dark gray, and black filled circles indicate, respectively, the relative locations of maser features during 2006 September–2007 February, 2009 May, and 2019 March cited from Paper III, Paper II, and the present work. The plus symbol is the same as in figure 3.

This scenario was also considered in figure 13 of Paper I, but was not favored there due to its inconsistency with the apparent systematic variation of the LSR velocities of the maser features along the outflow. However, Tafoya et al. (2019, 2020) proposed a more plausible model of a bipolar outflow, which is composed of a faster collimated jet and slower lobes surrounding the jet. They suggested that H_2O masers are excited in the lobes formed in the material entrained by the jet. Although we see a very rapid expansion of the whole maser distribution by ~140 mas in 13 yr, the
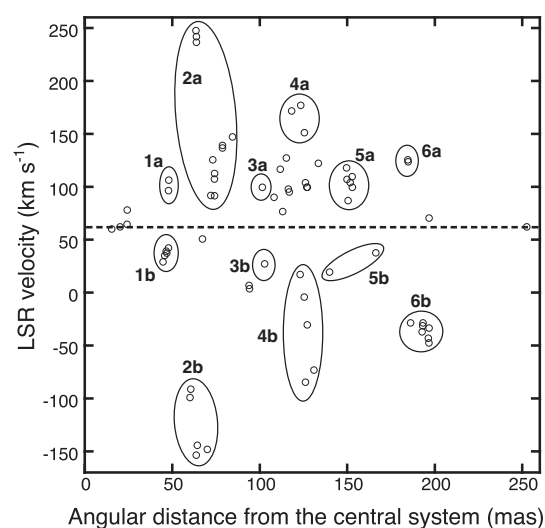
Fig. 5. Distribution of the maser features in IRAS 18286−0959 in a velocity–distance diagram. The LSR velocity against the distance from the central stellar system, assumed to be at $(X, Y) = (-43, 66)$ [mas], is displayed for each maser feature. A horizontal dashed line shows the assumed systemic velocity of the central stellar system, $V_{LSR} = 65$ km s^{-1}. The labels of the maser feature groups (from 1a/b to 6a/b) are the same as in figure 3.

expansion rate is consistent with the mean of the maser feature proper motions (8–10 mas yr^{-1}; Papers I, II, III). Thus, we are likely watching the evolution of the I18286 jet traced by the H_2O masers (section 4).

Figure 5 shows the distribution of the maser features in a velocity–distance diagram, suggesting episodic gas ejections traced by the H_2O masers. Taking into account the spacing between the groups of maser components (20–30 mas) and the mean maser proper motions (8–10 mas yr^{-1}), the time difference between the eruptions is roughly estimated to be 2–4 yr. The mean LSR velocity of the maser feature group pairs (1a/b, 3a/b, 5a/b) is derived to be ~75 km s^{-1}. Although the deviation of the mean velocity from the systemic velocity ($\Delta V \sim 10$ km s^{-1}) will provide a clue to the kinematics of the central stellar system, it should be examined in future thermal line mapping observations such as those made with ALMA.

Unfortunately, the highest-velocity components seen in our single-dish monitoring campaign ($V_{LSR} \approx 336$ and 345 km s^{-1}) could not be detected in the KaVA session. On the other hand, thanks to the precise astrometry of KaVA, we determined the absolute coordinates of the maser feature containing the position-reference maser spot at $V_{LSR} = 139.5$ km s^{-1}: RA(J2000, 0) = 18^{h}31^{m}22^{s}93440 ± 0^{s}00002, Dec(J2000.0) = −09°57′21″6654 ± 0″0003. This is useful for future precise registration between the maser emission and other spectral line maps.

4 Discussion

The previous single-dish observations in 2006 April–2010 April (Paper I) did not detect the new extremely high velocity components ($V_{LSR} < -60\,\mathrm{km\,s^{-1}}$ and $V_{LSR} > 200\,\mathrm{km\,s^{-1}}$) reported in this paper, with a 5σ upper limit to 0.57 Jy, which suggests that these components would appear after 2010 April. We note that the velocity coverage of our VERA and VLBA observations (22 epochs in total during 2006 September–2009 September; Papers I, II, III) did not cover the velocity ranges including the new components, and therefore we cannot ascertain whether such extreme components existed during those observations. One may wonder whether the material now showing extreme-velocity maser components was ejected much before their maser emission could be excited. However, this is unlikely. The material ejected at the expected initial speed ($>300\,\mathrm{km\,s^{-1}}$) would interact within 1–2 yr of the ejection with the ambient gas that excites the maser features located within a few tens of au ($\sim10\,\mathrm{mas}$) of the stellar system (Paper III). The travel time of the ejected material to arrive at the present positions would be only 5 yr or less.

The absence of the extreme components before 2010 (Paper I) should indicate the absence of the gas corresponding to these maser components at that time. Yung et al. (2013) found new velocity components in 2011 around $V_{LSR} \sim -90$ and $230\,\mathrm{km\,s^{-1}}$. However, the absence of information on their locations makes it difficult for us to suggest that they were also associated with the same gas clumps as those hosting our discovered maser components. In fact, there is a relatively large shift ($>10\,\mathrm{km\,s^{-1}}$) between the extreme-velocity components in Paper I and those in this paper.

Previous observations could have missed the high-velocity components (< -60 and $>200\,\mathrm{km\,s^{-1}}$) if their lifetime was short, as seen in the case of the components at 336 to $345\,\mathrm{km\,s^{-1}}$ and -178 to $-144\,\mathrm{km\,s^{-1}}$ in this paper. However, the components around -90 to -70 and 230 to $250\,\mathrm{km\,s^{-1}}$ are actually relatively stable, as seen in our monitoring observations, so we consider these components as a product of a new ejection after 2010 April. Here we propose that the stable high-velocity components seen at present would have formed soon after 2010 April with much higher velocities, like those seen in the unstable velocity components observed in 2019 February and May (or the 336 and $345\,\mathrm{km\,s^{-1}}$ components). If this is the case, they could already have been quenched during the rapid deceleration of the jet, while the most extreme components in this paper would be excited by a new, more recent, jet eruption.

We note here the colocation of the extreme velocity components in the southern side of the maser pair 2a and 2b with the components that have much lower velocities and flared flux densities in Group 4a (figure 3). This is also consistent with the scenario suggested by Tafoya et al. 2020, in which a new jet is interacting with the ambient, slower material that is then accelerated as entrained material along the jet. However, any physical relationship between the extreme velocity and flared components, including information on their relative locations along the line of sight, should be examined with further kinematic information.

On the other hand, as shown in figure 3, we can see a point-symmetric pattern in the distributions of maser feature groups with respect to the central stellar system. This implies recurrent maser activity with a period of 2–4 yr (subsection 3.2) or longer, together with recurrent gas eruptions. Taking into account the present size of the maser distribution ($\sim260\,\mathrm{mas}$ in the largest distance from the central stellar system) and its growth rate (8–$10\,\mathrm{mas\,yr^{-1}}$), the launching of the jet traced by H_2O is estimated to have happened in the year 1990 ± 7 years. Note also the existence of low-velocity components ($25 < V_{LSR} < 105\,\mathrm{km\,s^{-1}}$) that are located closer to the central system than the new components, such as a pair of maser features (1a and b in figure 3) and others possibly associated with the relic AGB envelope (Paper III). It is possible to consider that a pair of bipolar gas ejections may host not only the pair of the maser features mapped in this paper such as 2a and 2b, but also the fastest velocity components identified in single-dish spectra, but that are missing in this map. Similarly to the estimate described in subsection 3.2, and as supposed above, one can consider that gas clumps hosting these most extreme velocity, short-lived components were ejected within 2–4 yr of the present day.

We also consider here another scenario for the I18286 jet, where a jet has been launched at a projected expansion velocity of $\sim280\,\mathrm{km\,s^{-1}}$ as seen in the short-lived most extreme velocity components, which then decelerated to $\sim110\,\mathrm{km\,s^{-1}}$ as seen in the stable components detected over the last 10 yr due to drag by the ambient material in the CSE. This model is similar to that presented for I18113 by Orosz et al. (2019). Adopting an inclination angle of $\sim30°$, these projected expansion velocities correspond to $\sim330\,\mathrm{km\,s^{-1}}$ and $\sim130\,\mathrm{km\,s^{-1}}$, respectively. The jet velocity v is now expressed as $v(t) = v_0(1 + v_0 k t)^{-1}$, where v_0 is the initial velocity of the jet, k the coefficient of the exponential decay of the expansion velocity as a function of the mass density of the CSE, the mass of the individual jet clumps, the drag coefficient of the jet clumps, and the cross-sectional area of the jet clumps. We adopt $v_0 = 330\,\mathrm{km\,s^{-1}}$, $v(t) = 130\,\mathrm{km\,s^{-1}}$. When inserting $t \sim 30\,\mathrm{yr}$ as the dynamical age of I18286 (total length divided by the growth rate of the outflow estimated from the maser locations and proper motions), k is derived to be $\sim4.9 \times 10^{-17}\,\mathrm{cm^{-1}}$, which is well consistent with the

value derived for IRAS 18113−2503 ($k \sim 6.4 \times 10^{-17} \mathrm{cm}^{-1}$; Orosz et al. 2019).

However, one should remember the absence of the fastest maser features ten years ago and take into account the possibility that such components had already been decelerated to the velocity of the stable components ($\sim 110 \mathrm{km\,s^{-1}}$) within 10 yr. In this case we get a much larger k value, and a velocity drift of over $10 \mathrm{km\,s^{-1}\,yr^{-1}}$ should be observed and easily confirmed by weekly monitoring observations of the maser spectrum with a velocity resolution better than $1 \mathrm{km\,s^{-1}}$. In our present work, we could not confirm such extremely fast velocity drifts due to the sparseness of the monitoring observations. On the other hand, we can see a general trend in which the whole maser distribution seems to exhibit accelerations from Group 1a to 6a and from 1b to 6b (figure 4). Note that the distant maser features have an angular offset in the radial ejection direction from that of the closer and higher-velocity components. A possible explanation for the distant features is that they are moving more slowly in a less dense region of the outer CSE and therefore without the strong deceleration suggested for the high-velocity components. This is possible if we consider the precession of the jet. The first ejections have cleared up the CSE along the jet major axis, so that later ejections along that direction would travel more smoothly and with less deceleration than the highest-velocity ejections we see now along a different direction.

Paper I suggested the existence of twin jets, although it is unclear whether they are driven by a single stellar component or individual components in a stellar binary. The present results do not support that the twin jets are precessing anti-clockwise. This is evident when comparing the overall maser feature distributions over a decade, as shown in figure 4. Even with this rough superposition of the maser maps as described in subsection 3.2, it is clear that some of the representative pattern of the maser features such as arcs have been moving radially from the dynamical center at a rate of $\sim 10 \mathrm{mas\,yr^{-1}}$, as expected from the speed of the jet projected on the sky ($\gtrsim 150 \mathrm{km\,s^{-1}}$; Papers I, II, III). The maser distribution seems to have been growing in the western and eastern sides in the north-west and south-east lobes, respectively, suggesting clockwise jet precession and lobe development.

Nevertheless, it is noteworthy that the dynamical ages of the twin jets modeled in Paper I were different by ~ 10 yr. Interestingly, the value of this time lag roughly corresponds to 2–3 cycles of the possibly repeating outbursts. Thus, it is possible that some of the outbursts of a single jet could be further enhanced with a longer period, as mentioned, so as to form arc-shaped structures of maser distribution as seen in I18113 (Orosz et al. 2019).

In I18286, even with a single jet, enhanced periodic outburst, if they exist, may form maser distributions that apparently look like twin jets as illustrated in figure 14 of Paper I. The model simulations by Velázquez et al. (2012) also reproduce multiple bipolar lobes produced by a precessing bipolar jet from a binary system. Although those models focused on planetary nebulae with nebular lobe lengths of $\sim 10^4$ au and binary orbital periods of ~ 10 yr, one can consider a closer binary system for the case of I18286. We hope that the morphological evolution of the H_2O masers will be further elucidated in the next decade, enabling us to compare it with that predicted by the models, in order to derive the physical parameters of the jet and the possible binary system.

5 Conclusions

The spectroscopic monitoring in FLASHING and the VLBI follow-up imaging with KaVA of the H_2O masers in I18286 have revealed newly excited, extremely high velocity components in the H_2O masers and corresponding axisymmetric ejections of gas in the water fountain outflow. In this paper we have discussed the possibility that the stellar system driving the outflow has developed its outflow lobes with a wide opening angle through periodic gas ejections with a clockwise precession of the outflow axis, rather than through highly collimated twin jets with an anti-clockwise axis precession. The new model explains the observed maser feature distributions biased to the downstream sides of the bipolar lobes, namely the western and eastern sides of the northern and southern lobes, respectively.

Further VLBI monitoring observations of the new components of H_2O masers will enable us to find their decelerations, suggested by Tafoya et al. (2019, 2020), as a result of interactions between the ambient material and the entrained material around the high-speed jet. Thus, the combination of single-dish maser monitoring programs with targeted follow-up VLBI mapping observations provides an effective approach to investigating the ejection characteristics of water fountain jets/outflows. If the individual features in a variety of PN shapes are related to the individual events of such ejection behaviors seen in maser observations, this kind of approach will provide essential insights into the final stages of stellar evolution.

New ejections of the jet in I18286 should again be detected within several years if they are recurrent with time separations of 2–4 yr, as predicted by the spacing between maser groups. Since the size of the central binary system is expected be only a few au (e.g., Velázquez et al. 2012), which may correspond to a few mas or smaller, it is challenging to spatially resolve the system into a thermal collimated jet from the driving star and an equatorial disk/torus driving the jet, even with state-of-the-art instruments such as ALMA. Therefore, H_2O masers mapped with VLBI provide unique probes to elucidate the spatio-kinematical

information and possible periodic behavior of the central stellar system and the jet in I18286.

Acknowledgment

References

Chong, S. N., Imai, H., & Diamond, P. J. 2015, ApJ, 805, 53

Claussen, M., Sahai, R., & Morris, M. R. 2009, ApJ, 691, 219

Deguchi, S., Nakashima, J., Kwok, S., & Koning, N. 2007, ApJ, 664, 1130

Engels, D., & Bunzel, F. 2015, A&A, 582, A68

Gómez, J. F., et al. 2015, ApJ, 799, 186

Gómez, J. F., Rizzo, J. R., Suárez, O., Miranda, L. F., Guerrero, M. A., & Ramos-Larios, G. 2011, ApJ, 739, L14

Gómez, J. F., Suárez, O., Rizzo, J. R., Uscanga, L., Walsh, A., Miranda, L. F., & Bendjoya, P. 2017, MNRAS, 468, 2081

Herman, J., & Habing, H. J. 1985, A&A, 59, 523

Imai,, H. 2007, in IAU Symp. 242, Astrophysical Masers and their Environments, ed. W. Baan & J. Chapman (Cambridge: Cambridge University Press), 279

Imai, H., He, J.-H., Nakashima, J., Ukita, N., Deguchi, S., & Koning, N. 2009, PASJ, 61, 1365

Imai, H., Kurayama, T., Honma, M., & Miyaji, T. 2013a, PASJ, 65, 28   (Paper II)

Imai, H., Nakashima, J., Deguchi, S., Kwok, S., & Diamond, P. J. 2013b, ApJ, 773, 182

Imai, H., Nakashima, J., Yung, B. H. K., Deguchi, S., Kwok, S., & Diamond, P. J. 2013c, ApJ, 771, 47   (Paper III)

Imai, H., Obara, K., Diamond, P. J., Omodaka, T., & Sasao, T. 2002, Nature, 417, 829

Imai, H., Sahai, R., & Morris, M. 2007, ApJ, 669, 424

Lewis, B. M. 2001, Nature, 560, 400

Likkel, L., Morris, M., & Maddalena, R. J. 1992, A&A, 256, 581

Okada, N., et al. 2020, PASJ, 72, 7

Orosz, G., et al. 2019, MNRAS, 482, L40

Sahai, R., & Trauger, J. 1998, AJ, 116, 1357

Sahai, R., Vlemmings, W. H. T., Gledhill, T., Sánchez Contreras, C., Lagadec, E., Nyman, L.-Å., & Quintana-Lacaci, G. 2017, ApJ, 835, L13

Tafoya, D., et al. 2020, ApJ, 890, L14

Tafoya, D., Orosz, G., Vlemmings, W. H. T., Sahai, R., & Pérez-Sánchez, A. F. 2019, A&A, 629, A8

Velázquez, P. F., Raga, A. C., Riera, A., Steffen, W., Esquivel, A., Cantó, J., & Haro-Corzo, S. 2012, MNRAS, 419, 3529

Vlemmings, W. H. T., Diamond, P. J., & Imai, H. 2006, Nature, 440, 58

Yung, B. H. K., Nakashima, J., Imai, H., Deguchi, S., Diamond, P. J., & Kwok, S. 2011, ApJ, 741, 94 (Paper I)

Yung, B. H. K., Nakashima, J., Imai, H., Deguchi, S., Henkel, C., & Kwok, S. 2013, ApJ, 769, 20